

CHANDRA DETECTS A RAPID FLARE IN THE GRAVITATIONALLY LENSED
MINI-BALQSO RX J0911.4+0551

G. CHARTAS¹, X. DAI¹, S. C. GALLAGHER¹, G. P. GARMIRE¹, M. W. BAUTZ²,
P. L. SCHECHTER², AND N. D. MORGAN²

The Astrophysical Journal, accepted

ABSTRACT

The mini Broad Absorption Line (BAL) quasar RX J0911.4+0551 was observed with the Advanced CCD Imaging Spectrometer (ACIS) of the *Chandra X-ray Observatory* for ~ 29 ks as part of a gravitational lens (GL) survey aimed at measuring time-delays. Timing analysis of the light-curve of the lensed image A2 shows a rapid flux variation with a duration of about 2000s. A Kolmogorov-Smirnov test shows that the probability that a constant-intensity source would produce the observed variability is less than $\sim 0.2\%$. We discuss possible origins for the observed short-term X-ray variability. Our gravitational lens models for the RX J0911.4+0551 GL system predict a time-delay of less than a day between images A1 and A2. The rapid variability combined with the predicted short-time delay make RX J0911.4+0551 an ideal system to apply the GL method for estimating the Hubble constant. We describe the prospects of measuring H_0 within single X-ray observations of GL systems with relatively short time delays. Modeling of the spectrum of the mini-BAL quasar RX J0911.4+0551 suggests the presence of an intrinsic absorber. Partial covering models are slightly preferred over models that contain absorption due to intrinsic ionized or neutral gas.

Subject headings: gravitational lensing: individual (RX J0911.4+0551) – X-rays: general – quasars: individual (RX J0911.4+0551) – quasars: (BAL)

1. INTRODUCTION

Even before the discovery of the first gravitational lens system by Walsh et al. (1979) it was realized by Refsdal (1964) that measurements of the light travel time difference between lensed images may provide an estimate of the Hubble constant. More recently it was shown that measurements of the time-delay can provide the absolute distance to the intervening deflector independent of cosmological parameters such as H_0 , Ω_m and Ω_Λ (Narayan, 1991). Significant observational and modeling efforts made since then have revealed that the application of Refsdal's method and the uncertainties involved are more complex than originally anticipated.

The main difficulty in measuring time-delays is that the brightness of each image has to be carefully monitored, continually over several periods of the time-delay. Also, the quasar has to show sufficient variability over time-scales smaller than the time-delay. Most attempts to measure time-delays until now have been made in the optical and radio bands. The modest variability of quasars in these wave-bands, however, has made it extremely difficult to place accurate constraints on time-delays. To add to this complexity,

microlensing by stars in the lensing galaxy may produce variability on time-scales of the order of weeks to years. Microlensing variability of this kind does not lead to a time-delayed signal between the lensed images thus complicating timing analysis.

It has also become apparent from the extensive modeling of several well-studied GL systems, such as Q0957+561 (Bernstein and Fisher, 1999), that a large range of potential models for lenses can satisfy the available observable constraints thus contributing to the large uncertainty in present estimates of the Hubble constant based on Refsdal's method. X-ray observations of gravitationally lensed quasars may alleviate some of the complexities associated with obtaining accurate time delays while achieving this goal in a fraction of the time and monitoring effort. However, X-ray observations of lensed quasars, have been very limited until recently due to the relatively low spatial resolution and collecting area of X-ray telescopes (Chartas, 2000). Since the launch of the *Chandra X-ray Observatory* on 1999 23 July, however, the X-ray sky can now be imaged at 0.4 arcsec resolution and the field of gravitational lensing has suddenly become available to the high energy astrophysics community.

¹Astronomy and Astrophysics Department, Pennsylvania State University, University Park, PA 16802., chartas@astro.psu.edu

²MIT Center for Space Research, 70 Vassar Street, Cambridge, MA, 02139.

The first realization of the possibility of measuring short time delays came with the *Chandra* observation of the distant $z = 2.8$ quasar RX J0911.4+0551. The main lens of this system is a galaxy at a redshift of 0.769 (Falco, Davis & Stern, 1999, private communication). A cluster of galaxies has been detected at about 38 arcsec SW from RX J0911.4+0551 at the same mean redshift of 0.7692 ± 0.004 (Kneib et al. 2000) and is thought to contribute to the lensing of the quasar. The X-ray image and a deconvolved image of RX J0911.4+0551 are presented in a companion paper by Morgan et al. (2001).

Optical spectra of RX J0911.4+0551 obtained by Bade et al. (1997) show an absorption trough bluewards of the C IV associated resonance line that spans a velocity range of about 3200 km s^{-1} . Absorption features of similar nature have been observed in approximately 10% of optically selected quasars and are attributed to highly ionized gas flowing away from the central source. Quasars observed to contain such absorption systems are commonly referred to as Broad Absorption Line quasars (Turnshek et al. 1988; Weymann et al. 1991). The relatively small velocity spread observed in RX J0911.4+0551 compared to the typical range of $5,000 \text{ km s}^{-1} < v < 25,000 \text{ km s}^{-1}$ observed in BAL quasars suggest that RX J0911.4+0551 be classified as a mini-BAL quasar (Turnshek 1988, Barlow, Hamann, & Sargent 1997).

The analysis presented in the following sections focuses on the variability of the light-curves and spectra of the lensed images of RX 0911.4+0551. The paper is structured as follows: In section 2 we describe the timing analysis of the *Chandra* observation of RX J0911.4+551, and in section 3 we present estimates for short time-delays in GL systems with small image separations. The spectral analysis of the lensed images is presented in section 4. We conclude in section 5 with a summary of our results and a discussion of the prospects of constraining cosmological parameters by applying the short time delay method.

2. TIMING ANALYSIS

A description of the *Chandra* observation of RX J0911.4+0551 is presented in a companion paper by Morgan et al. (2001). An elementary study of the combined light-curve of images A1 and A2 indicates a significant variation of the X-ray flux within a period of about 2 ks. Resolving the closest imaged pairs A1 and A2 (0.48 arcsec separation) of the GL system RX J0911.4+0551 is just within the capabilities of the *Chandra*/ACIS combination. Observations of the source PG1634-706 during the orbital calibration phase of the mission demonstrated that on-axis observations, corrected for aspect and spacecraft dither, can produce 50% encircled energy radii

of about 0.42 arcsec. The observed 50% encircled energy radius for image B of RX J0911.4+0551 is ~ 0.38 arcsec. To search for variability in the individual images A1 and A2 we extracted light-curves from rectangular regions with sides of length $\Delta ra = 2$ arcsec and $\Delta dec = 0.8$ arcsec centered on the centroids of the images as determined from the deconvolution analysis described in Morgan et al., (2001). The light-curves of images A1 and A2 are shown in Figure 1. The time resolution for this observation is 3.241sec. The light-curves in Figure 1 are binned in 1166.76s intervals, and are corrected for background events. Background is estimated by extracting events from a neighboring source-free region. The binned light-curves show a flare occurring in image A2 and not image A1. Two consecutive data points in the light-curve of image A2 lie at $\sim 3\sigma$ above the mean value. The duration of the X-ray flare is ~ 2000 s and the count-rate changed from ~ 5 counts per bin to ~ 15 counts per bin. The background flares that occur at several intervals during the observation do not coincide with the 2000s interval where we detect variability in A2.

The background rate during the X-ray flare is $\sim 6 \times 10^{-6}$ events $\text{s}^{-1} \text{ pixel}^{-1}$ (including only events with *ASCA* grades 0,2,3,4,6 and with energies within 0.5-8keV). For the A2 source region the number of background counts expected during the 2000s X-ray flare in A2 is ~ 0.007 counts.

More appropriate and unbiased tests for unbinned data of this nature are the Kolmogorov-Smirnov (K-S) and Kuiper tests. In Figure 2 we show the cumulative probability distribution versus exposure time for the light-curves of A1 and A2. We find a significant deviation in A2, with a chance probability of about 1.8×10^{-3} for the K-S test applied to the entire duration of the observation. Results for the Kuiper test are similar and are presented in Table 1. Since the X-ray flare in image A2 occurs over a brief period of ~ 2000 s we expect that the K-S probability applied over the entire observation of A2 may be a conservative value, however, we expect it to be unbiased with respect to time filtering. We also applied to K-S test over several narrower time intervals containing the flare. The results are shown in Table 1. The K-S probabilities for these time intervals range from 3.2×10^{-4} to 2.3×10^{-5} and indicate a high significance for the presence of a flare in image A2 but not in image A1.

An aspect error could mimic a sudden increase in the observed count-rate in a small extraction region. We rule this out since an increase in X-ray flux is still present for extraction regions that include all lensed images. Also such an aspect error would produce variability in the light-curve of image A1, that is not

observed. Remaining plausible causes of variability are the quasar, its environment and microlensing. We discuss these cases in section 4.

3. SHORT TIME DELAYS

The time delay between two images with an angular separation of $\Delta\theta$ scales roughly as $\sim \Delta\theta^2$. Extrapolating from optical and radio measurements of time-delays we expect that time-delays in several systems with $\Delta\theta < 0.5$ arcsec to range between hours to days.

To obtain more accurate estimates of the short time delays for individual systems with small angular separations we modeled these using the χ^2 minimization method of Kayser et al. (1990) and Kochanek (1991).

We chose a variety of lens potentials to investigate the sensitivity of estimated short time delays to the mass distribution of the lens and to evaluate the feasibility of observing these delays with the *Chandra X-ray Observatory* and *XMM-Newton*. To account for the presence of a cluster of galaxies centered ~ 38 arcsec SW of RX J0911.4+0551 we have included a shear component in our models. Shear measures the anisotropic stretching of the image and is due to mass residing outside the beam (Weyl focusing).

The adopted two-dimensional projected potentials are,

$$\psi_{PMXS}(\vec{\theta}) = b^2 \ln r + \frac{\gamma}{2} r^2 \cos[2(\theta - \theta_\gamma)] \quad (1)$$

$$\psi_{ISXS}(\vec{\theta}) = br + \frac{\gamma}{2} r^2 \cos[2(\theta - \theta_\gamma)] \quad (2)$$

$$\psi_{ISEP}(\vec{\theta}) = br + \gamma br \cos[2(\theta - \theta_\gamma)] \quad (3)$$

where PMXS represents a point mass with external shear model, ISXS describes an isothermal sphere with external shear model, and ISEP considers an isothermal elliptical potential model. In the equations above, r and θ are polar coordinates of the image with respect to the galaxy, γ is the shear, θ_γ is the orientation of the shear (measured from North to West), and b is the strength of the lens.

$$b = 4\pi \frac{D_{ls}}{c^2 D_{os}} v_{G0}^2 \quad (4)$$

where v_{G0} is the velocity dispersion of the galaxy, D are the angular diameter distances, and the subscripts l, s, and o refer to the lens, deflector and observer (see Schechter et al. 1997 and references within for more details on these lens models). The time delay between an image at a position $\vec{\theta}$ and an unlensed light path is

$$\tau(\vec{\theta}) = \frac{(1+z_d)}{c} \frac{D_d D_s}{D_{ds}} \left[\frac{1}{2} (\vec{\theta} - \vec{\beta})^2 - \psi(\vec{\theta}) \right]$$

where $\vec{\beta}$ is the source position. The observable constraints are the positions of the lensed images and deflector galaxies taken from the CfA-Arizona Space Telescope LENS Survey (CASTLES) of gravitational lenses website <http://cfa-www.harvard.edu/glensdata/>. The best fit parameters obtained by minimizing the χ^2 statistic formed between observables and their modeled values are listed in Table 2. We find that in many GL systems with small-image separations the time-delays are less than a day making them suitable for short-time delay measurements with the *Chandra* and *XMM-Newton* observatories. Specifically, for RX J0911.4+0551 (Table 3) we find that the best fit model (model ISXS in Table 3) yields a time-delay value of $0.65h^{-1}$ days between images A1 and A2 and $0.46h^{-1}$ days between images A1 and A3. The detection of a flare in A2 and not in A1 constrains the time-delay between these images to be greater than 23 ks, consistent with our model results. The best fit value for the position angle of the external shear for the ISXS model is PA = 187deg. This is close to the observed position angle of PA ~ 197 deg of X-ray emission from the lensing cluster (see Morgan et al. 2001). Considering the additional complexity introduced by the presence of a cluster of galaxies in the lens plane further detailed modeling of this system is needed.

4. SPECTRAL ANALYSIS

The spectra for images A1, A2, and A3 were extracted from circular regions centered on images with radii of 0.25 arcsec. The spectrum of image B was extracted from events within a 1 arcsec circular region centered on B. The background was determined by extracting events within an annulus centered on A1 with inner and outer radii of 10 arcsec and 15 arcsec, respectively. We also created a spectrum combining all lensed images extracting events within a circular region centered on A1 with a radius of 10 arcsec. Since the source spectra were in units of PHA, the data from nodes 0 and 1 are extracted and analyzed separately in order to account for gain differences between the amplifiers. The parameters for each data set were linked together for the model fitting with the exception of the absolute normalization.

A simple power-law model with neutral cold absorbers at $z=0$ was used to estimate a photon spectral index Γ for the combined spectrum. Throughout the X-ray spectral analysis, the Galactic absorption is fixed at $N_H = 3.6 \times 10^{20} \text{ cm}^{-2}$. We initially restricted the fit to only include events with energies above 1.32keV (5 keV rest frame). By restricting the fit to these energies we can infer the underlying power-law continuum component and avoid possible biasing towards harder spectra in the event that

additional absorption by neutral or partially ionized gas is present. We find a best fit value for $\Gamma = 1.91_{-0.34}^{+0.39}$ typical of radio-quiet quasars at high redshifts (e.g., Brandt, Mathur & Elvis 1997; Reeves & Turner 2000), and $\chi^2=11.6$ for 9 degrees of freedom. Extrapolating this best fit model to lower energies reveals a significant residual suggesting the presence of intrinsic absorption. The resulting plot, shown in the Figure 3, is suggestive of the possible nature of the intrinsic absorber. The spectra appear to recover towards the power-law continuum in the lowest energy bins, hinting at either partially ionized absorbing gas or partial covering of the continuum. In contrast, a neutral, cold absorber would depress almost all flux below ≈ 5 keV, the energy where the continuum recovers.

We fit several models to try to characterize the absorbing gas. The details of each fit are listed in Table 4. Briefly, intrinsic absorption by neutral gas at $z = 2.8$ with column density $3.4 \times 10^{22} \text{ cm}^{-2}$ was preferable at the $> 95\%$ confidence level to a straight power law with only absorption fixed to the Galactic value of $3.6 \times 10^{20} \text{ cm}^{-2}$ according to the F -test ($\Delta\chi^2 = -5.6$). In addition, adding neutral intrinsic absorption resulted in a photon index of $\Gamma = 1.57_{-0.29}^{+0.36}$ which is much closer to the value of $\Gamma = 1.91$ for the fit to the data above 5 keV in the rest frame than the value of $\Gamma = 1.25$ for the fit that did not include intrinsic absorption. However, the residuals still showed some systematic effects, in particular, a positive excess in the 5–11 keV (1.3–3.0 keV observed frame) range.

We also considered models with absorption placed at the redshift of the lensing galaxy (see Table 4). We find no significant change in χ^2 compared to fits that include intrinsic absorption. We conclude that our spectral analysis cannot constrain the redshift of the absorber. In a latter part of this section, based on the observed properties of intrinsic absorbers in RX J0911.4+0551 (Bade et al. 1997), we present physical arguments that imply that the most likely origin of absorption in excess of the Galactic value is the immediate quasar environment. We, therefore, restrict the spectral analysis that follows to models that consider intrinsic absorption.

Fitting the data with a warm absorber or a partial covering model also yielded acceptable fits to the data and gave reasonable photon indices (see Table 4); the partial covering model was slightly preferred at the 63% confidence level over the neutral absorber model (see figure 4). Absorption of some kind is certainly required, however, the low signal-to-noise ratio of the data (the combined spectrum of all images contains a total of 425 X-ray events) preclude a determination of the specific nature of the absorber. Recent

X-ray gratings analyses of the warm absorber in the Seyfert galaxy NGC 3783 (Kaspi et al. 2000) and the absorption in the QSO IRAS 13349+2438 (Sako et al. 2001) indicate that those absorbers are more complex than the simple one-zone photoionization models typically used to model CCD-resolution data. Given that RX J0911.4 is a luminous mini-BAL QSO, complex X-ray absorption is not unreasonable.

We searched for differential extinction in the spectra of the lensed images. Because of the low signal-to-noise we kept the spectral photon index fixed to the value of 2.0 and assumed Galactic and intrinsic absorption due to cold gas at the quasar redshift. The results of these fits are presented in Table 5. We find that the intrinsic column density of images A1, A2, and B is similar and of the order of $\sim 5 \times 10^{22} \text{ cm}^{-2}$. Due to the low signal-to-noise of A3 it is not possible to constrain the column density towards the line of sight to this image within a useful bound.

The quantity $\alpha_{\text{ox}} = -\frac{\log(f_X/f_{\text{opt}})}{\log(\nu_X/\nu_{\text{opt}})}$, the spectral index of a power law defined by the flux densities at rest-frame 3000Å and 2 keV, is a useful parameter for measuring the X-ray power of a QSO relative to its ultraviolet continuum emission. A large, negative α_{ox} indicates relatively weak soft X-ray emission; the mean value of α_{ox} for radio-quiet AGN is ≈ -1.48 (e.g., Laor et al 1997) with a typical range from -1.7 to -1.3 (e.g., Brandt, Laor & Wills 2000). Weakness in soft X-rays is plausibly explained by intrinsic X-ray absorption, which strongly decreases the observed flux at the lowest energies. A strong correlation of large, negative values of α_{ox} with the absorption-line equivalent width of C IV supports this hypothesis (Brandt, Laor, & Wills 2000). As expected, BAL QSOs populate the extreme end of this correlation: they are the weakest soft X-ray sources as well as the QSOs with the most extreme ultraviolet absorption. Recent spectroscopic observations of two AGN with strong C IV absorption, PG 1535+547 and the BAL QSO PG 2112+059, found direct evidence of intrinsic X-ray absorption causing strongly negative values of α_{ox} (Gallagher et al 2001).

Given the observed C IV absorption-line equivalent width of RX J0911.4+0551, $EW_{\text{ABS}} = 4.4\text{\AA}$ (Bade et al. 1997) and our calculated α_{ox} we compare this mini-BAL QSO with QSOs in the Brandt, Laor & Wills (2000) correlation. Specifically, we extrapolate the observed rest-frame ultraviolet continuum from Bade et al. (1997) to 3000Å (rest frame), and apply the best-fitting X-ray model from our spectral analysis to obtain the 2 keV (rest frame) flux density. We find an observed $\alpha_{\text{ox}} = -1.72$ and corrected for absorption, $\alpha_{\text{ox}} = -1.52$, consistent with the value for normal, unabsorbed AGN. RX J0911.4+0551 thus fits coherently within the correlation of Brandt, Laor

& Wills (2000). Given that the C IV absorption is undoubtedly intrinsic from the velocity spread, $\delta V \approx 3200 \text{ km s}^{-1}$, and redshift of the absorbers (Bade et al. 1997), identifying the X-ray absorption as intrinsic, rather than at the redshift of the lens, provides the most reasonable physical explanation for the X-ray spectral modeling.

To obtain additional clues of the origin of the X-ray flare we estimated the hardness ratio of image A2 during the X-ray flare state and the quiescent state. For the purpose of this analysis we define as the X-ray flare state the time interval between 7.2 and 9.2 ks from the beginning of the observation and as quiescent state the remaining period of the observation. The hardness ratio is defined as the counts in the 1.3–8.0 keV band divided by the counts in the 0.5–1.3 keV band. We find that the hardness ratio changed from 1.45 ± 0.34 in the quiescent state to 0.67 ± 0.27 in the flare state. If the flare resulted from a decrease in the intrinsic, absorbing column density, then the hardness ratio would decrease as the number of counts in the soft band increased. The estimated hardness ratio for a $\Gamma = 1.9$ power-law with only Galactic absorption (and no intrinsic absorption) is ~ 0.6 . Correlations of spectral slope with X-ray flux have been observed in Seyfert galaxies. In particular, a strong correlation of spectral slope with UV flux and broad-band X-ray flux have been observed in the Seyfert 1 galaxies NGC 7469, NGC 5548 and IC4329a (Nandra, 2000; Chiang et al. 2000; Done, Madejski & Zycki 2000). In the Comptonization model (Haardt, Maraschi & Ghisellini 1997; Zdziarski, Lubinski & Smith 1999) an increase of the seed UV photons leads to an increase of the Compton upscattered X-ray photons and a cooling of the disk corona, resulting in a softened X-ray spectrum. Another plausible explanation for the change in hardness ratio could arise with partial covering of the quasar by an intrinsic absorber. Partial covering could result from lines of sight through the absorber combined with unobscured lines of sight off a scatterer (eg. Gallagher et. 2001). The spectrum of the unobscured emission will be softer than that of the absorbed emission. If the unobscured emission is scattered into the line of sight then the path-lengths between the X-ray source and us will be different for the unobscured and absorbed components. We therefore expect a delay between the arrival of these components. A sudden flare of the quasar could thus result in a variation of the hardness ratio. Specifically, the hard absorbed component of the flare will reach us first followed by the scattered softer component. It is the sudden increase in the scattered component that we propose as the origin of the softening of the spectrum of RX J0911.4+0551 during the flare.

5. DISCUSSION AND CONCLUSIONS

Micro lensing, a phenomenon induced by the random motion of stars in the lensing galaxies of GL systems has been proposed as the cause of observed wavelength-dependent variability in lensed images of QSO 2237+0305 (Woźniak et al. 2000). The short duration and shape of the X-ray flare in image A2 of RX J0911.4+0551 rule against a microlensing event. Observed microlensing events have typical time-scales of weeks to years. Microlensing can produce variations in the observed flux of a lensed object when the characteristic length scale of the emitting region is comparable to the projected Einstein-ring radius, $\zeta_E = [(4GM/c^2)(D_{os}D_{ls}/D_{ol})]^{1/2}$, produced by a star of mass M in the lens plane, where D represents the angular diameter distances, and the subscripts l , s , and o refer to the lens, source, and observer, respectively. For the GL system RX J0911+0551 with lens and source redshifts of $z_{lens} = 0.769$ and $z_{source} = 2.8$ respectively, and assuming an isolated star of mass M the Einstein-ring radius on the source plane is $\zeta_E \sim 0.01 (M/M_\odot)^{1/2}$ pc. The expected duration of a microlensing event is approximately equal to the time for the source to cross an Einstein-ring radius. Assuming the transverse velocity of the source with respect to the caustic network is $v_l = 1000 \text{ km s}^{-1}$, the time-scale of the microlensing event is $t_E = \zeta_E/v_l \sim 11 \text{ yr}$.

A more rapid variation, occasionally referred to as a high magnification event (HME), is expected to occur during a caustic crossing. Witt, Mao & Schechter (1994) estimate the rise time of such an event as $t_{HME} \sim 3.3(r_s/v_l)$, where r_s is the characteristic length scale for the source emission region. For an X-ray emission region of $r_s = 10^{-4}$ pc and for projected source velocities ranging between 1000 km s^{-1} and 100 km s^{-1} the expected rise time for a HME event is $t_{HME} \sim 0.3 - 3 \text{ yr}$. We conclude that a caustic crossing is very unlikely to have produced the X-ray flare.

Having ruled out instrumental effects and microlensing as the cause of the rapid flare in RX J0911.4+0551 we discuss plausible mechanisms related to the quasar and its environment. Correlations of spectral variability of AGN with X-ray luminosity have been observed in a number of AGN (eg, Nandra 2000, and references therein). In particular, these studies indicate a strong anti-correlation between variability amplitude and X-ray luminosity. For example, Seyfert galaxies with 2-10 keV luminosities ranging between 10^{42} - $10^{44} \text{ erg s}^{-1}$ show significantly larger variability amplitudes than quasars with 2-10 keV luminosities ranging between 10^{45} - $10^{47} \text{ erg s}^{-1}$. RX J0911.4+0551 has an unlensed 2-10 keV luminosity of $L_X \sim 5 \times 10^{44} \text{ erg s}^{-1}$, where we have

assumed a magnification factor of 20 (see Table 3). Based on the observed dependence of variability amplitude with luminosity we expect RX J0911.4+0551 to exhibit variability comparable to that seen in Seyferts.

Assuming that the cause of the detected 2000s X-ray flare is intrinsic to the quasar we place a rough estimate on the size of the emitting region of about $d \sim ct = 1.5 \times 10^{-4}$ pc (corrected for time-dilation). Note that due to the low signal-to-noise we may have just detected the peak of the flare, thus the true duration of the flare may be slightly longer than observed. To estimate the accuracy of measuring the time-delay between images A1 and A2 we simulated light-curves for these lensed images with fluxes similar to those observed and added Poisson noise. Figure 5 shows simulated light-curves for images A1 and A2. The intensity of the X-ray flare in A2 is normalized to that measured in the Chandra observation of RX J0911.4+0551. The simulated X-ray flare in A1 is shifted with respect to the flare in A2 by $t_{delay} = 75$ ks. The count-rate in the non-flare regions of the light-curves was set to the observed value of $\sim 4 \times 10^{-3}$ cts s^{-1} . The cross-correlation function of the light-curves of images A1 and A2 is shown in Figure 5. A time-delay of 75 ks is clearly recovered in the cross-correlation function. A Monte-Carlo realization of this simulation indicates that the percent fractional error in the recovered time-delay is $\sim 1.5\%$ (95% confidence). We estimated the significance of the cross-correlation peak value of 0.3 by performing a Monte-Carlo simulation for a constant source model, assuming a count-rate value of $\sim 4 \times 10^{-3}$ cts s^{-1} . We find the probability of obtaining a cross-correlation peak value of 0.3 or greater for a constant source model to be less than $\sim 1 \times 10^{-6}$. Our simple simulations, based on the observed rapid flare and the predicted short time-delay, suggest that measurements of a time-delay in the GL system RX J0911.4+0551 with an accuracy of about 1% is possible within a single observation with the *Chandra* or *XMM-Newton* X-ray observatories. Time-delays can also be extracted from light-curves of unresolved images via autocorrelation techniques as long as the fluxes of the two images are similar. Measurements of accurate short time-delays may be possible in eight additional X-ray bright GL systems based on the predictions of our lensing models for these systems (see Table 2). The potential usefulness of X-ray observations of GL systems can be appreciated if one considers that it has taken almost 20 years of optical and radio monitoring to obtain a universal accepted time-delay for GL quasar Q0957+561 to an accuracy of $\sim 1\%$. X-ray observations of short time-delay systems offer the prospect of providing the same accuracy within 1-2

days of observing time. In quadruple systems with measured long time-delays, obtained from monitoring in the optical and/or radio bands (see Fassnacht et al. 1999), the addition of accurate short - time delays can provide additional constraints on the gravitational potential of the lens, thus providing tighter constraints on the Hubble constant.

Our spectral analysis of the mini-BAL quasar RX J0911.4+0551 is suggestive of softening of the X-ray spectrum during the flare state. A plausible explanation, based on Compton upscattering models, is that the softening of the X-ray spectral slope during the flare is produced by cooling of the disk corona as a result of an increase in UV seed photons in the accretion disk. A different explanation that is consistent with our spectral analysis is the scattering of an unabsorbed soft component in addition to the direct absorbed one. A delay in arrival between the absorbed and scattered components may explain the observable variation in the hardness ratio. Spectral fits that include intrinsic absorption due to cold gas are preferred at the ($> 95\%$) confidence level over ones that only include Galactic absorption. A highly ionized absorber at the redshift of RX J0911.4+0551 is also acceptable in a statistical sense with best fit values of the ionization parameter and column density of 300 erg cm s^{-1} and 1×10^{23} atoms cm^{-2} respectively. Partial covering models are slightly preferred over neutral and ionized absorber ones with a best fit covering fraction of $0.7_{-0.39}^{+0.2}$. Spectral modeling of the individual images A1, A2, and B suggests no evidence for significant differential extinction. Due to the low signal to noise in image A3 it is not possible to constrain the intrinsic column density within a useful bound.

We would like to thank E. Feigelson for helpful discussions related to unbiased tests of variability. We acknowledge financial support by NASA grant NAS 8-38252. SGC gratefully acknowledges the support of NASA GSRP grant NGT5-50277.

TABLE 1
TESTS OF VARIABILITY OF RX J0911.4+0551

Test	Time Interval	Statistic		Chance Probability	
		A2	A1	A2	A1
K-S	0—29.6 ks	0.18	0.05	1.8×10^{-3}	0.78
Kuiper	0—29.6 ks	0.23	0.09	3.9×10^{-4}	0.57
K-S	1—28.6 ks	0.20	0.05	3.2×10^{-4}	0.81
Kuiper	1—28.6 ks	0.23	0.10	5.7×10^{-4}	0.46
K-S	2—27.6 ks	0.23	0.07	5.2×10^{-5}	0.43
Kuiper	2—27.6 ks	0.25	0.11	1.2×10^{-4}	0.27
K-S	3—26.6 ks	0.25	0.06	2.7×10^{-5}	0.59
Kuiper	3—26.6 ks	0.26	0.12	2.1×10^{-4}	0.29
K-S	4—25.6 ks	0.26	0.08	2.3×10^{-5}	0.44
Kuiper	4—25.6 ks	0.27	0.14	2.7×10^{-4}	0.10

TABLE 2
GRAVITATIONALLY LENSED SYSTEMS
WITH PREDICTED SHORT TIME DELAYS

Object	Image Separation arcsec	Time-Delay ($h^{-1}days$)
RX J0911.4+0551	0.47(A1-A2)	0.65(ISXS)
PG 1115+080	0.48(A1-A2)	0.065(ISXS), 0.16(SIE)
MG 0414+0534	0.42(A1-A2)	0.35(ISXS)
APM 08279+5255	0.15(A-C)	0.19(ISXS)
B1422+231	0.51(A-B)	0.09(ISXS), 0.37(SIE)
2237+0305	1.0(A-D)	0.14(SIE)
B0712+472	0.16(A-B)	0.05(SIE)
B0218+357	0.00137(A1-A2)	<0.01(SIE)
1608+656	0.88(A-C)	0.85(ISXS),1.9(SIE)

NOTES-

Time-Delays are estimates based on fitting gravitational lens models to the observable image positions. We have considered isothermal sphere plus external shear (ISXS), and singular isothermal ellipse (SIE) potentials. The time-delays determined using SIE models are taken from the CfA-Arizona Space Telescope LEns Survey (CASTLES) of gravitational lenses website <http://cfa-www.harvard.edu/glensdata/>.

TABLE 3
 MODEL PARAMETERS, TIME DELAYS AND MAGNIFICATIONS FOR LENS MODELS OF RX J0911.40551

Model	x (arcsec)	y (arcsec)	b (arcsec)	γ	θ_γ (deg)	A1-A2 h^{-1} days	A1-A3 h^{-1} days	A1-B h^{-1} days	M_{A1}	M_{A2}	M_{A3}	M_B	χ^2_ν/ν
PMXS	-0.649	0.064	1.028	0.5	172.64	-0.92	1.78	-147.92	-2.42	1.60	-0.72	1.09	5.11/3
ISXS	-0.433	0.047	1.108	0.31	173.00	-0.65	0.46	-105.86	-6.51	8.41	-2.78	1.78	0.50/3
ISEP	-0.666	0.069	1.368	0.15	172.23	-0.53	1.19	-149.19	-5.85	4.43	-1.88	1.50	7.88/3

NOTES-

PMXS represents a point mass with external shear model, ISXS describes an isothermal sphere with external shear model, and ISEP considers an isothermal elliptical potential model. γ is the shear, θ_γ is the orientation of the shear (measured from North to West), and b is the strength of the lens. M represents the best fit values for the magnifications of the lensed images A1, A2, A3 and B. x and y are the best fit positions of the source with respect to the lensing galaxy. The positions of the lensed images and deflector galaxies used to derive the lens parameters are taken from the CASTLES website <http://cfa-www.harvard.edu/glensdata/>.

TABLE 4
SPECTRAL FITTING PARAMETERS FOR THE COMBINED SPECTRUM
OF IMAGES RX J0911+0551 A1, A2, A3 and B^a

Model	Γ	Parameter Name	Value ^b	χ^2/ν	$P(\chi^2/\nu)$
Power Law (PL)	$1.25^{+0.14}_{-0.15}$	28.7/20	0.095
PL, $E > 5$ keV rest frame (1.32 keV observed frame)	$1.91^{+0.39}_{-0.34}$	11.6/9	0.24
PL with intrinsic, neutral absorption	$1.57^{+0.36}_{-0.29}$	$N_{\text{H}}(10^{22} \text{ cm}^{-2})$	$3.4^{+2.6}_{-3.1}$	23.1/19	0.23
PL with neutral absorption at lens	$1.61^{+0.28}_{-0.28}$	$N_{\text{H}}(10^{22} \text{ cm}^{-2})$	$0.55^{+0.46}_{-0.36}$	22.6/19	0.25
PL with intrinsic, partial-covering absorption ^c	$1.87^{+0.98}_{-0.66}$	$N_{\text{H}}(10^{22} \text{ cm}^{-2})$	$19.0^{+27.9}_{-17.7}$	21.5/18	0.26
		Coverage fraction	$0.71^{+0.20}_{-0.39}$		
PL with intrinsic, ionized absorption ^c	$1.6^{+0.5}_{-0.4}$	$N_{\text{H}}(10^{22} \text{ cm}^{-2})$	10^{+33}_{-9}	23.2/18	0.23
		ξ	$300^{+>300}_{-300}$		
PL with ionized absorption at lens ^c	$1.78^{+0.5}_{-0.4}$	$N_{\text{H}}(10^{22} \text{ cm}^{-2})$	$2^{+2.4}_{-1.6}$	21.8/18	0.24
		ξ	80^{+120}_{-80}		

NOTES-

^aAll model fits include fixed, Galactic absorption, $N_{\text{H}} = 3.72 \times 10^{20} \text{ cm}^{-2}$ (Schlegel et al. 1998).

^bThe errors are for 90% confidence with all parameters taken to be of interest except absolute normalization.

^cThe parameters for this model are poorly constrained, and so all parameters other than Γ have 68% confidence errors.

TABLE 5
 MODEL PARAMETERS DETERMINED FROM SPECTRAL FITS TO THE
 INDIVIDUAL SPECTRA OF IMAGES OF RX J0911.4+0551

Fit ^a	Image	Γ	$N_H(z=0)$ 10^{22} cm^{-2}	$N_H(z=2.8)$ 10^{22} cm^{-2}	Flux ^b	χ^2_ν/ν
1(0.3-6.keV)	A1+A2+A3+B	2.0(fixed)	0.037(fixed)	$5.1^{+1.94}_{-1.46}$	$5.2^{+0.2}_{-0.2}$	1.71/21
1(0.3-2.9keV)	A1	2.0(fixed)	0.037(fixed)	$4.4^{+2.65}_{-1.95}$		1.41/14
2(0.3-2.9keV)	A2	2.0(fixed)	0.037(fixed)	$5.1^{+3.88}_{-2.62}$		1.20/8
3(0.5-2.9keV)	A3	2.0(fixed)	0.037(fixed)	$1.2^{+13}_{-1.2}$		1.6/3
4(0.2-2.9keV)	A3	2.0(fixed)	0.037(fixed)	$0.2^{+2.2}_{-0.2}$		1.54/4
5(0.3-2.9)	B	2.0(fixed)	0.037(fixed)	$3.6^{+3.1}_{-1.9}$		0.2/2

NOTES-

^a The spectral fits were performed within the energy ranges listed in the parentheses.

^b Flux is estimated in the 2-10keV band as is in units of 10^{-14} erg $\text{s}^{-1} \text{ cm}^{-2}$

REFERENCES

- Barlow, T. A., Hamann, F., & Sargent, W. L. W. 1977, in ASP Conf. Ser. 28, Mass Ejection from AGN, ed. N. Arav, I. Shlosman, & R. J. Weymann, (San Francisco:ASP), 13
- Bernstein, G. & Fischer, P., 1999, AJ, 118, 14
- Brandt, W.N., Mathur, S., & Elvis, M. 1997, MNRAS, 285, L25
- Brandt, W. N., Laor, A., & Wills, B. J., 2000, ApJ, 528, 637
- Burud, I., Courbin, F., Lidman, C., Jaunsen, A. O., Hjorth, J., Ostensen, R., Andersen, M. I., Clasen, J. W., Wucknitz, O., Meylan, G., Magain, P., Stabell, R. and Refsdal, S., 1998, ApJ, 501, L5
- Chartas, G., 2000, ApJ, 531, 81
- Chiang, J., Reynolds, C. S., Blaes, O. M., Nowak, M. A., Murray, N., Madejski, G., Marshall, H. L. & Magdziarz, P., 2000, ApJ, 528, 292
- Done, C., Madejski, G. M., & Zycki, P. T., 2001, ApJ, in press
- Fassnacht, C. D., Pearson, T. J., Readhead, A. C. S., Browne, I. W. A., Koopmans, L. V. E., Myers, S. T., Wilkinson, P. N., 1999, ApJ, 527, 498
- Gallagher, S. C., Brandt, W. N., Laor, A., Elvis, M., Mathur, S., Wills, B. J. and Iyomoto, N., 2001, ApJ, 546, 795
- Haardt, F., Maraschi, L., & Ghisellini, G., 1997, ApJ, 476, 620
- Kaspi, S., Brandt, W.N., Netzer, H., Samburina, R., Chartas, G., Garmire, G. P. & Nousek, J. A. 2000, ApJL, 535, L17
- Kayser, R., Surdej, J., Condon, J. J., Kellermann, K. I., Magain, P., Remy, M. and Smette, A., 1990, ApJ, 364, 15
- Kneib, J., Cohen, J. G., & Hjorth, J., 2000, ApJ, 544, L35
- Kochanek, C. S., 1991, ApJ, 373, 354
- Laor, A., Fiore, F., Elvis, M., Wilkes, B. J., & McDowell, J. C. 1997, ApJ, 477, 93
- Morgan, N. D., Chartas, G., Malm, M., Bautz, M. W., Jones, S. E., and Schechter, P. L., 2001 submitted to ApJ.
- Narayan, R., 1991, ApJ, 378, L5
- Nandra, K., 2000, to appear in Advances in Space Research, astro-ph/0012448
- Refsdal, S., 1964, MNRAS, 128, 295
- Reeves, J. & Turner, M. 2000, MNRAS, 316, 234
- Sako, M. et al. 2001, A&A, in press (astro-ph/0010660)
- Schechter, P. L. , Bailyn, C. D., Barr, R., Barvainis, R., Becker, C. M., Bernstein, G. M., Blakeslee, J. P., Bus, S. J., Dressler, A., Falco, E. E., Fesen, R. A., Fischer, P., Gebhardt, K., Harmer, D., Hewitt, J. N., Hjorth, J., Hurt, T., Jaunsen, A. O., Mateo, M., Mehlert, D., Richstone, D. O., Sparke, L. S., Thorstensen, J. R., Tonry, J. L., Wegner, G., Willmarth, D. W. and Worthey, G., 1997, ApJ, 475, L85
- Turnshek, D. A., Foltz, C. B., Grillmair, C. J., & Weymann, R. J., 1988, ApJ, 325, 651
- Walsh, D., Carswell, R. F., & Weymann, R. J., 1979, Nature, 279, 381
- Weymann, R. J., Morris, S. L., Foltz, C. B., & Hewitt, P. C., 1991, ApJ, 373, 23
- Witt, H. J., Mao, S., and Schechter, P. L., 1995, ApJ, 443, 18
- Woźniak, P. R., Alard, C., Udalski, A., Szymański, M., Kubiak, M., Pietrzyński, G., and Zebruń, K., 2000, ApJ, 529, 88
- Zdziarski, A., A., Lubinski, P., & Smith, D. A., 1999, MNRAS, 303, L11

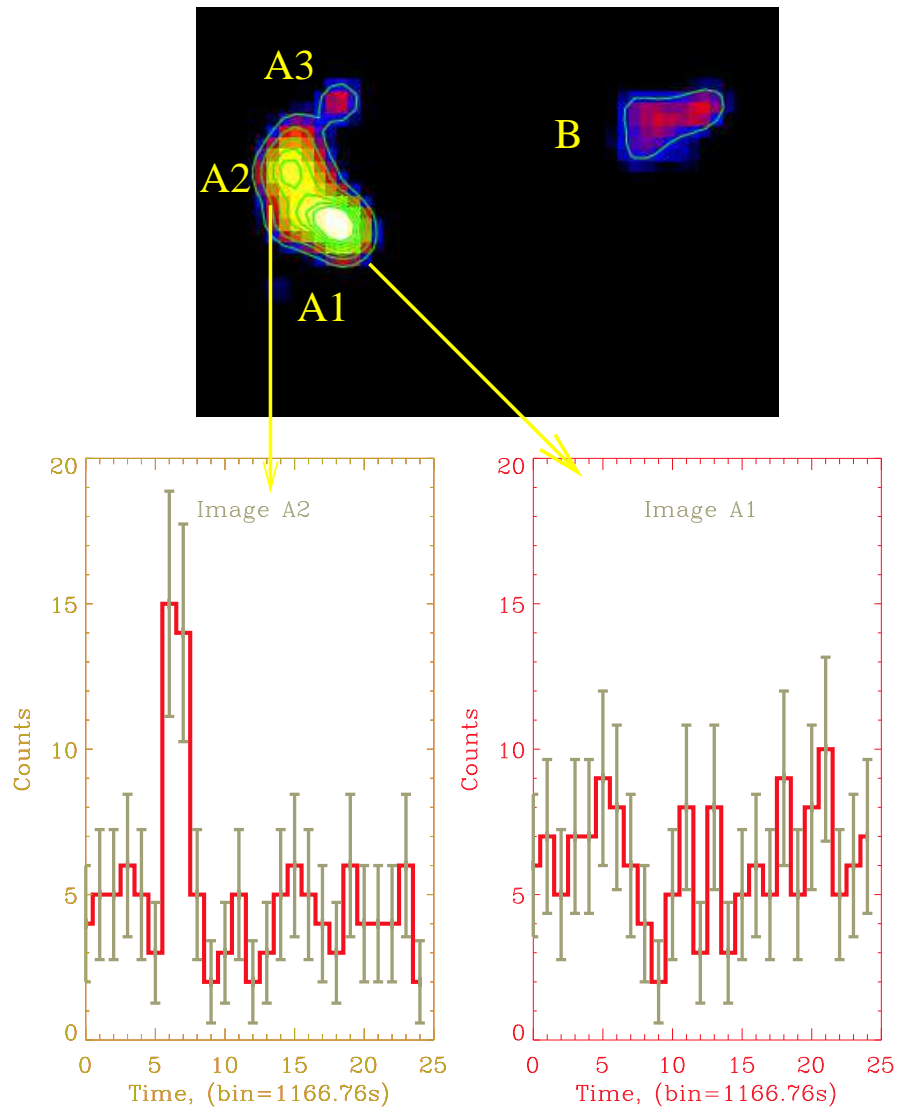


FIG. 1.— This figure is a composite of the deconvolved X-ray image of the gravitational lens RX J0911.4+0551 (top panel) and the light-curves of the lensed images A2 (left panel) and A1 (right panel). *Chandra* clearly resolves the four lensed images of the distant quasar. A rapid flare that lasted for about 2000s was recorded in image A2 whereas image A1 does not show any variability.

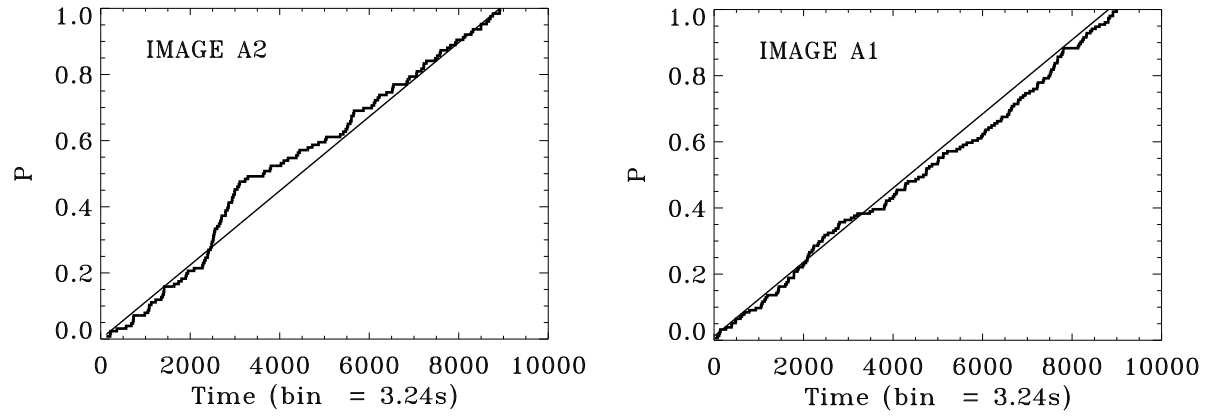


FIG. 2.— Cumulative probability distribution versus exposure number for image A2 (left panel) and image A1 (right panel) compared to the cumulative probability distribution of a constant source.

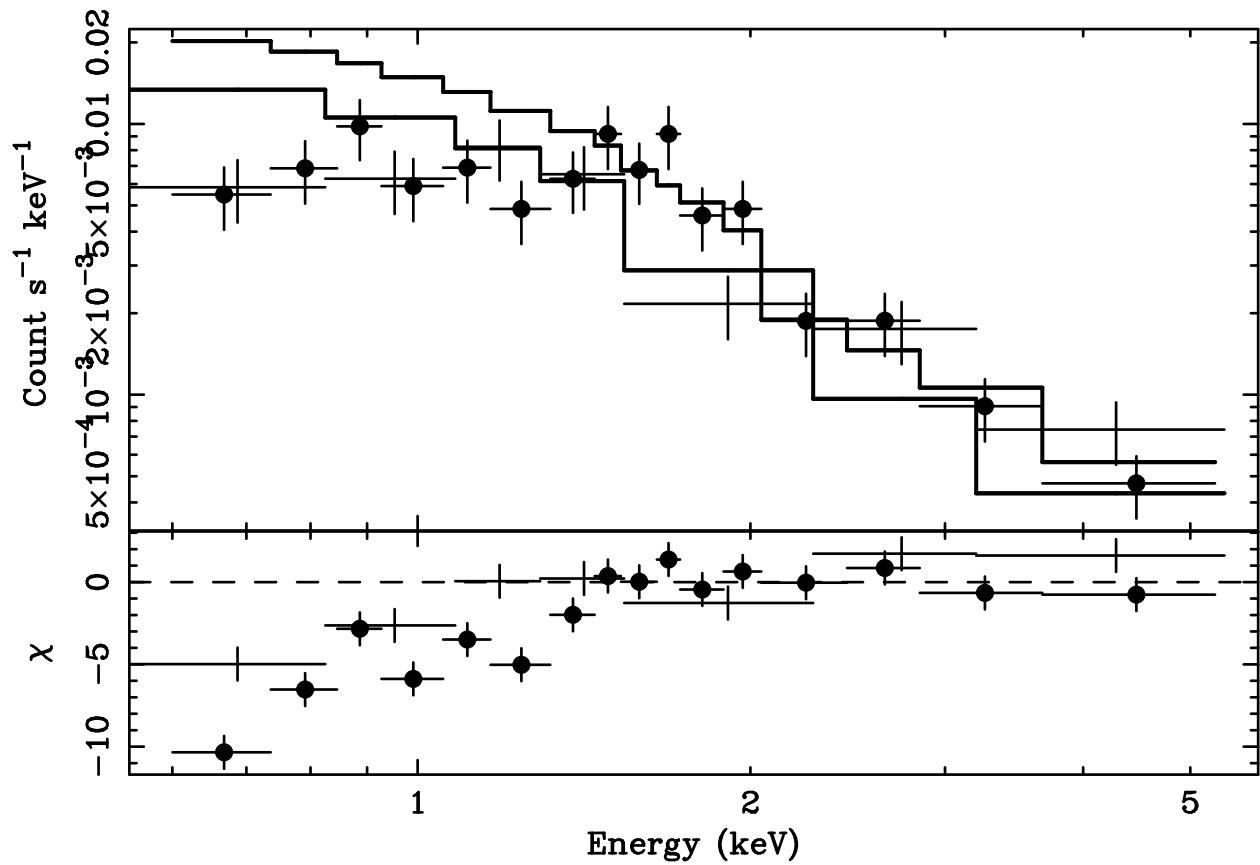


FIG. 3.— *Chandra* observed-frame spectra of the combined A1, A2, A3, and B images fit with Galactic absorption and a power-law model above 1.3 keV (5 keV rest frame) that is then extrapolated back to lower energies. Filled circles are the data points from node 0 while plain crosses represent the data points from node 1. The ordinate for the lower panel, labeled χ , shows the fit residuals in terms of σ with error bars of size one. Note that the flux in the lowest energy bins is not completely extinguished. This suggests the absorber is ionized, partially covering the continuum, or both.

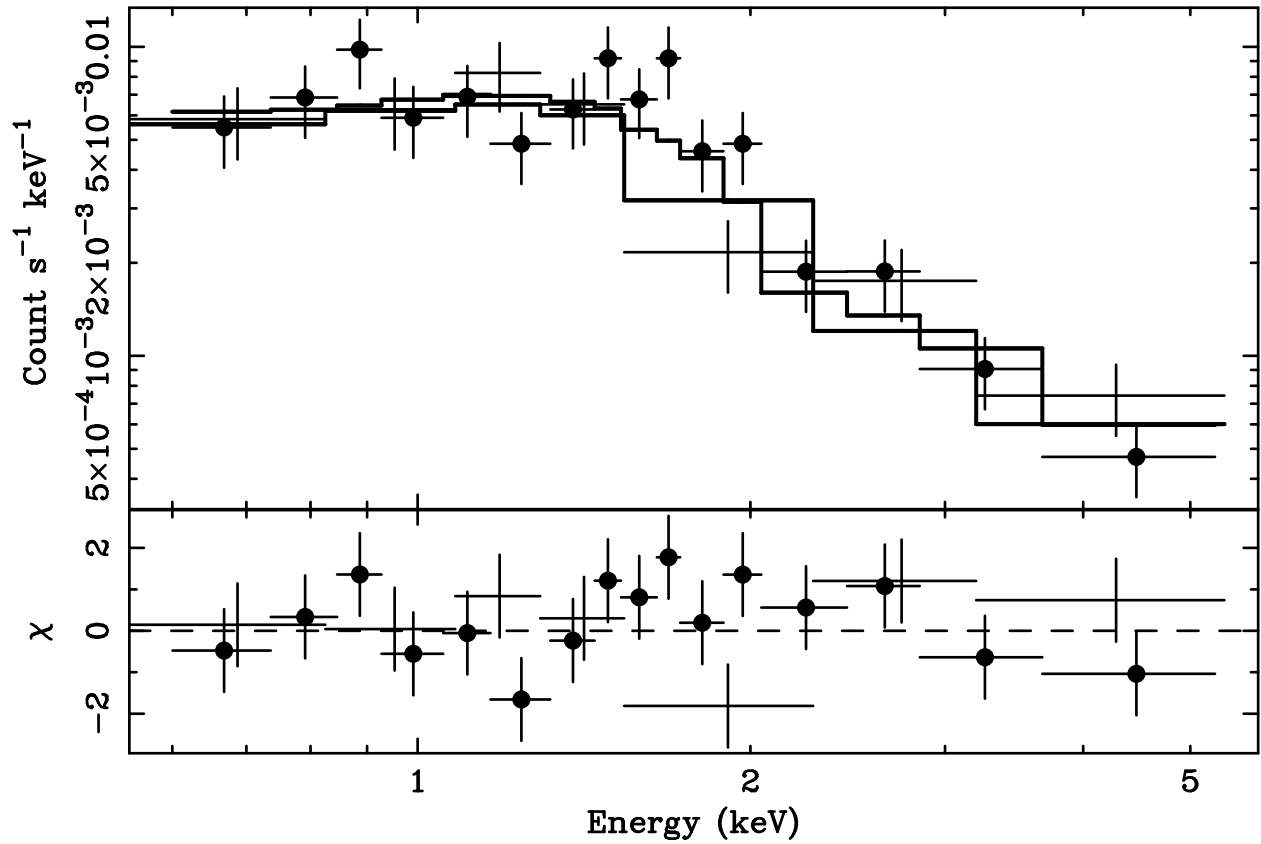


FIG. 4.— *Chandra* observed-frame spectra of the combined A1, A2, A3, and B images fit with a power-law model, partially covering intrinsic absorption, and Galactic absorption. Filled circles are the data points from node 0 while plain crosses represent the data points from node 1. The ordinate for the lower panel, labeled χ , shows the fit residuals in terms of σ with error bars of size one. This model provides an acceptable fit to the data that is a statistically significant improvement over intrinsic warm or neutral absorption. In addition, the photon index ($\Gamma = 1.9$) is consistent with the hard band ($E > 5$ keV) power law (Figure 3) and the range for radio-quiet QSOs.

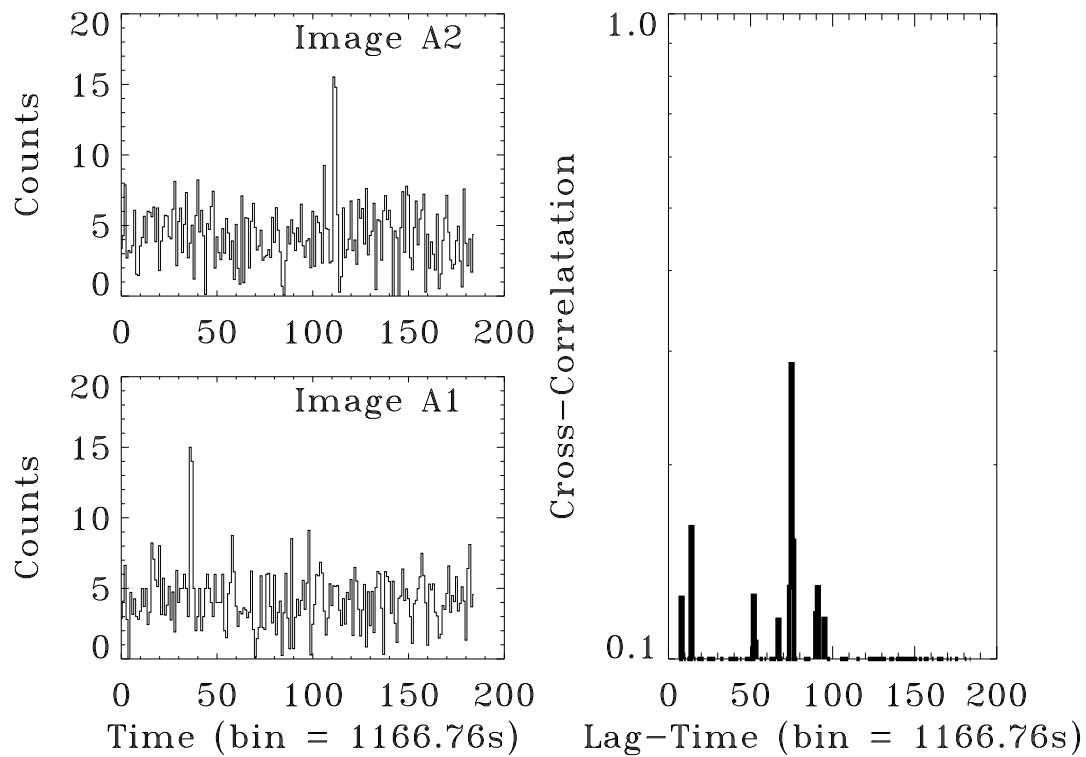


FIG. 5.— Simulated light-curves for images A1 and A2 of RX J0911.4+0551 (left panels) with cross-correlation function (right panel). The simulated light-curves of the flare and non-flare regions are based on the *Chandra* observations of RX J0911.4+0551. The input delay was set at the predicted value of 75 ks. The cross-correlation of light-curves A1 and A2 clearly resolves the 75 ks time-delay.